# TECHNICAL MEMORANDUM

## X-394

# THE AMES ATMOSPHERE ENTRY SIMULATOR AND ITS APPLICATION TO THE DETERMINATION OF ABLATIVE PROPERTIES OF MATERIALS FOR BALLISTIC MISSILES

By Frank M. Hamaker

Ames Research Center
Moffett Field, Calif.





NATIONAL AERONAUTICS AND SPACE ADMINISTRATION
WASHINGTON
October 1960

NATIONAL AERONAUTICS AND SPACE ADMINISTRATION

TECHNICAL MEMORANDUM X-394

# THE AMES ATMOSPHERE ENTRY SIMULATOR AND ITS APPLICATION TO THE DETERMINATION OF ABLATIVE PROPERTIES OF MATERIALS FOR BALLISTIC MISSILES*

By Frank M. Hamaker

## SUMMARY

The atmosphere entry simulator at the Ames Research Center is described. It is demonstrated that the motion and heating of long-range ballistic missiles can be simulated with small-scale models in this facility. Results are also presented of tests to determine the feasibility of ethyl cellulose plastic as an ablative material for long-range ballistic missiles. The test models consisted of spherically tipped cone cylinders of 0.788-inch diameter and tip radii equal to one-fourth the diameter. The cone half-angle was 50° and the models weighed 4.3 grams (0.0095 pound). The tests simulated the motion and heating of ballistic missiles with atmosphere entry velocities ranging from 10,000 to 21,500 feet per second, with diameters varying from 4.5 to 5.4 feet, with weights varying from 3150 to 5500 pounds, and with ranges varying from 640 to 4150 statute miles, respectively.

It was deduced that flow over the model was predominately turbulent at entrance velocities in excess of 14,000 feet per second. A relation is presented for the effective heat capacity of ablating materials in turbulent flow as a function of local enthalpy. This relation is employed in conjunction with the test results for the ablation weight losses to estimate the effective heat of ablation for ethyl cellulose.

The results of these tests indicate that ethyl cellulose retains its structural integrity under conditions which simulate re-entry thermal stresses. The percentage of the initial weight lost as a result of ablation varied from 0.5 percent at the lowest entry velocity to 2.6 percent at the highest velocity.

*Title, Unclassified

## INTRODUCTION

An important problem in the entry of long-range ballistic missiles into the atmosphere is the protection of the vehicles from the attendant severe aerodynamic heating. The fact that both the missile velocity and the atmosphere density vary with altitude is a complicating factor to any analysis.

The possibility of simulating the flight conditions of re-entry on a laboratory scale was first suggested by Eggers in reference 1. It was shown that the motion and heating of a ballistic missile could be simulated and that the total heat per unit mass and thermal-stress history of a heat-sink type of heat shield would be duplicated between model and missile. The motion and heating simulation was essentially verified by experiment in reference 2. In reference 3 it was shown that this simulation could be extended to the case where there is ablation from the nose of the vehicle.

In the present paper a large atmosphere entry simulator is described and the results are reported of tests therein to determine the pertinent characteristics of ethyl cellulose plastic as an ablation heat shield material for long-range ballistic missiles. Symbols are defined in appendix A.

## ATMOSPHERE ENTRY SIMULATOR

### Description of Equipment

Figure 1 is a schematic diagram of the atmosphere entry simulator. The apparatus consists of four main parts: pressure tank, test channel, vacuum sphere, and model launcher. The 17 cubic-foot pressure tank is separated initially from the test channel by a diaphragm which can be ruptured to allow the high-pressure air to flow through the test channel into an evacuated sphere of 18,000 cubic foot capacity. The test channel is a supersonic nozzle 40 feet long with a square cross section and a design exit Mach number of about 6.2. The minimum throat height of the nozzle is 5.04 inches located about 40 inches from the pressure tank, and the nozzle expands to a height of 5 feet 2-1/2 inches. The nozzle contour was designed to give an exponential variation in the air density along the channel; namely

$$\frac{\rho}{\rho_o} = e^{-\beta y} \tag{1}$$

where $\beta$ = constant and $y$ is the distance downstream from the pressure tank. In the 40-foot length of the test chamber, an altitude segment of the atmosphere of about 132,000 feet is simulated. The particular

segment can be chosen by selecting the appropriate initial pressure in the tank. A photograph of the tank and test channel is shown in figure 2.

There are 12 windows along each of the 4 walls of the test channel. At the downstream edge of each vertical window is a photobeam station consisting of a light source and a photoelectric tube on opposite sides of the channel. As the model passes each photobeam station, it intercepts the photobeam and the time increment is recorded by electronic counters. Shadowgraph systems are located at pertinent horizontal- and vertical-window stations. Figure 3 is a sketch of the optical arrangement of a typical shadowgraph system. Not shown is a shutter on the camera which was opened only during the flight of the model down the channel. This somewhat complex system was used to avoid overexposure of the shadowgraph picture by the muzzle flash of the model launcher. The spark light source for the shadowgraph picture is fired by a suitable time-delayed trigger circuit connected to the adjacent photobeam station. In addition to the spark exposure there may be a streak exposure due to luminescence in the region of the model. The example shadowgraph presented in figure 4 shows such a streak. The intensity of this streak can vary with model velocity and model material.

The models are launched upstream through the test channel by a two-stage shock-compression helium gun. The first shock tube is 4 inches in diameter and the helium inside is compressed by a powder charge in the breech. The shock wave formed in this tube reflects off a piston in the second tube which is 2-1/4 inches in diameter. The piston is driven down this tube at high speed, creating a very strong shock wave in the helium before it. The shock-compressed and -heated helium then drives the model down the 20 millimeter launch tube. A detailed discussion of the gun may be found in reference 4.

## Calibration of the Test Channel

Flow in the test channel was calibrated by means of static side-wall orifices and by static- and pitot-pressure probes mounted in the center line of the channel at four different stations. Static pressures, both side wall and center line, were measured by diaphragm capacitance gages and the pitot pressures were measured by strain-gage type transducers, except at very low pressures where capacitance gages were used. The output of the gages was recorded on cathode-ray oscillographs. These oscillograph records indicated that flow stabilized in 20 milliseconds after rupture of the diaphragm and the flow remained established in the tunnel for about 200 to 300 milliseconds, depending on the initial tank pressure. Calibrations were made for initial tank pressures of 105, 315, and 655 pounds per square inch absolute and with the air in the tank at room temperature.

The pressures were measured from the oscillograph records at 100 milliseconds after the rupture of the diaphragm. The pressures obtained were referenced to the reservoir pressure and used to determine the densities on the basis of one-dimensional isentropic-flow theory. Figure 5 shows the results of this calibration in which the ratio of local to reservoir densities has been plotted on a logarithmic scale so that the resulting data should lie on a straight line. The differences in the results due to the variation of initial tank pressure were within the experimental scatter of the data; hence, only averaged results are shown. In determining the best fit to the data greater weight was given to the center-line measurements. The resulting correlation yields a curve corresponding to $\beta = 0.15$ per foot. The design value for the nozzle was $\beta = 0.135$ per foot. The difference is similar to that found in the small simulator (ref. 2) and is probably due to the same causes; namely, an overcompensation for boundary-layer growth and error due to the one-dimensional flow assumption made in designing the nozzle.

## EXPERIMENTAL PROCEDURE

### Test Models

The models consist of a spherically tipped conical nose with a cylindrical afterbody, the dimensions of which are shown in figure 6. The nose of each model was compared to the same template so that the dimensions were the same for all models within 0.0001 inch. The afterbody was not maintained to such accuracy; therefore, each model was carefully weighed and the diameter and afterbody length was measured prior to testing. The average weight of the models was 4.3 grams.

The model material was blue ethocel which is a special grade of ethyl cellulose plastic manufactured by Dow Chemical Company. It is a hard, transluscent, dark-blue plastic with a very high impact strength.

### Test Procedure

All models were launched at approximately 80 milliseconds after rupture of the diaphragm and a time-distance history was determined from the data recorded on the electronic counters. Entrance velocities ranged from 10,000 to 21,500 feet per second relative to the air stream. The pressure in the reservoir tank was adjusted in each test to maintain a terminal velocity of approximately 1000 feet per second. At the end of their flight the models were recovered in sponge rubber. For

this purpose this material was found to be superior to balsa wood which was employed in the small simulator tests (ref. 3). The recovered models were then measured and weighed to determine their weight losses and any changes in dimensions.

## Data Reduction

The velocities of the models were calculated from the time-distance record. The photobeam stations near the muzzle of the model launcher did not function reliably; however, model velocity close to the launcher could be accurately determined by graphical extrapolation. The extrapolation method was based on an analytical solution to the equation of motion of the model relative to the channel. The development of this solution is given in appendix B.

The ablation weight loss was determined by subtracting the loss due to erosion in the gun barrel from the total weight loss. The weight lost on the sides of the models during launching was calculated from the density of the material and the changes in the diameter of the models. In general, the ablation caused about 60 percent of the total weight loss. An alternate method of determining ablation weight loss was considered in which a photograph of the magnified profile of the model was taken after testing and was compared with a template of the original profile. The loss in volume was calculated by graphical integration methods and the material density was then used to determine the weight loss. It was found that this method was no more accurate nor more reliable than the method used.

## Accuracy of the Data

The primary source of error in the time-distance history is the uncertainty in the location of the model at the time the photobeam triggers the counter. This could be treated either as a distance error or a time error and the resulting velocity error is estimated to be ±1.5 percent. The percentage error in the extrapolated muzzle velocity is slightly larger.

Because of the great accuracy with which models can be weighed, the error in the total weight loss was of the order of ±0.1 percent; however, it was in the weight loss due to launching, which was calculated from dimensional measurements, that the major error occurred. The critical dimension in determining the launching weight loss is the difference between the initial and the final diameters of the model. Because of the smallness of this dimension, its error may be as high as ±15 percent

even though linear measuring accuracies may be good to 0.0002 inch. The error in the volume change, and therefore in the weight loss, is the same as the above dimensional error, namely, ±15 percent. Since the launching weight loss is a smaller portion of the total weight loss than is the ablation weight loss, the error in the ablation loss will be somewhat less. Based on the 60-percent value given above, the error in the ablation weight loss is ±10 percent. This is an upper limit of the ablation weight error which becomes less for larger weight losses and may become as low as ±5 percent.

## RESULTS AND DISCUSSION

### Missile Simulation

A typical variation of velocity with simulated altitude for a test model is shown in figure 7. For comparison, the theoretical velocity variation for the simulated vehicle is also shown. The theoretical trajectory was based on the simulation criteria established in reference 1. The stagnation heat-transfer rate to the simulated missile is also shown in this figure and was calculated as suggested in reference 5. It should be noted here that the size of the missile simulated can be varied by assuming various entrance angles for the missiles. The entrance angle shown in figure 7 was prescribed as indicated in reference 6 by the requirement for maximum range for an entrance velocity of 20,200 feet per second. It is apparent from figure 7 that the requirement for simulation of equal velocities for model and missile at corresponding points in the trajectories was essentially satisfied. It is also clear that the major portion of the heating history of the full-scale vehicle fell within the range of the simulation tests. The results in this figure are typical of the test results in general.

In the table below there are given some representative missiles simulated by the present series of tests according to the requirement of maximum range for a given entrance velocity.

| Entry velocity, ft/sec | Entry angle, deg | Missile diameter, ft | Missile weight, lb | Maximum range, statute miles |
|---|---|---|---|---|
| 10,000 | 42.8 | 4.5 | 3150 | 640 |
| 14,000 | 40.1 | 4.6 | 3450 | 1190 |
| 19,000 | 34.2 | 5.0 | 4220 | 2980 |
| 21,500 | 29.2 | 5.4 | 5500 | 4150 |

## Ablation Simulation

The ablation mass losses on the models are shown for various entry velocities in figure 8 where the mass losses are presented as percentages of the initial mass of the model. As indicated, the maximum ablation loss was about 2.6 percent and occurred at an entry velocity of 21,500 feet per second. The application of these experimental results to the simulated full-scale vehicle was at least in part deterred by insufficient data on the properties of the material tested. As pointed out in the analysis presented in reference 3, however, the probable errors in model to missile ablation loss simulation are within experimental accuracy for materials of the type tested. Therefore, the experimental mass losses presented are also indicative of the mass losses to be expected on the simulated missiles. Analysis (ref. 1) has also shown that there is model to missile simulation of the thermal stresses imposed on the ablation material during entry. Since, for the present tests, the recovered models were free from cracks, it is indicated that this material could also withstand the thermal stresses encountered by the simulated missiles. On the basis of these results, then, ethyl cellulose would appear to be a reasonably efficient ablative material for long-range ballistic missiles.

## Evaluation of Flow Conditions on Surface

One of the basic criteria for the simulation just discussed was that model and missile have the same Reynolds number (see ref. 1). It therefore follows that model and missile should have the same flow conditions on the surface. The surfaces of the recovered models should have the same appearance and distribution of ablation as those on the simulated full-scale missiles. Their appearance should help predict whether laminar or turbulent flow predominated over the surface of the models. Prediction of the type of flow was necessary to evaluate local heating rates on the surface and, thus, to estimate the ablative properties of the material tested as will be discussed later.

Photographs of the surfaces of models recovered after flight at various entry speeds are shown in figure 9 along with a photograph of an unfired model. It should be noted that at the lowest test velocity the surface remained essentially smooth. For the intermediate velocity, the conical surface became wavy in appearance. At the highest velocity, the waviness had extended forward onto the spherical tip. This waviness may be related to the presence of turbulent flow on the surface.

Photographs are shown in figure 10 which compare the profiles of the ablated models with those of the original shape. These photographs were obtained by projecting the silhouette of a recovered model on the

ground glass of an optical comparator to which was affixed the template for the original model. For the low test velocity, it will be noted that the ablation loss was confined mainly to the stagnation region. Such a distribution of ablation loss would be consistent with laminar flow since, in this case, the highest heating rates would occur at the stagnation point. For the high test velocity, however, the ablation loss was greatest on the conical section. This distribution of ablation loss would be expected for turbulent flow since, in this case, the local heat-transfer rates would be greater than those at the stagnation point (see ref. 7).

It is indicated from figures 9 and 10, then, that, at the higher entry velocities, the simulated missile will have a wavy surface on the conical section of the nose and will have most of its material ablated from this region. From these indications, moreover, there is strong evidence that turbulent flow was the dominant factor in the ablation losses experienced at the higher test velocities.

The existence of turbulent flow over the conical region of the model was further inferred by another consideration. From the results presented in reference 8, it was concluded that, for the present tests, transition to turbulent flow would occur at a Reynolds number of about 0.5 million. Calculations have been made, therefore, to determine when the local Reynolds number on the model might exceed this value. For these calculations, the Reynolds number was evaluated at the spherical tangent point on the model and at the point of maximum heating in the trajectory. The results of these calculations are shown in figure 11. It can be seen that the expected transition Reynolds number of 0.5 million is exceeded for entry velocities greater than about 13,000 feet per second. Since, as shown in figure 7, maximum heating occurred considerably before maximum Reynolds number during the entry trajectory, it was considered highly probable that turbulent flow would exist over the conical region of the model during the time of entry after maximum heating. It was also evident that transition to turbulent flow could occur much before maximum heating at the higher entrance velocities.

From the various considerations made here, it was concluded that the presence of turbulent boundary-layer flow could be a predominate factor in the ablation losses measured from the tests at the higher entry velocities. Based on this conclusion, estimations were made of the effective heat of ablation for the test material.

## Estimation of Effective Heat of Ablation

It was assumed that ablation on these models took place, primarily at least, by vaporization. It should be noted from reference 3 that

when this is the case the effective heat of ablation and percent mass loss between model and simulated missile are essentially duplicated.

A subliming ablation process has been studied in reference 9 for laminar flow in which it was concluded that the effective heat of ablation was a function of the air enthalpy but not the heat-transfer rate and is given in rather simplified form as

$$H_{eff} = \frac{q_o}{w} = c_p T_v + h_v + \frac{2}{3} M^{1/4}(h_e - h_w) \qquad (2)$$

The first two terms on the right in this expression indicate the energy required to vaporize the material. The last term is a measure of the shielding effectiveness of the vapor. This last term was derived from a semiempirical correlation of laminar transpiration cooling results in the form

$$\frac{q_i}{q_o} = 1 - \frac{2}{3} \frac{M^{1/4} w(h_e - h_w)}{q_o} \qquad (3)$$

where $M$ is the ratio of the molecular weight of air to that of the injected vapor; $w$ is the mass injection or ablation rate; $q_o$ is the heat-transfer rate without mass injection at the ablation temperature; $q_i$ is the heat-transfer rate with mass injection; and $(h_e - h_w)$ is the enthalpy difference across the boundary layer.

A similar correlation of experimental results for turbulent transpiration cooling has been made (see appendix C) and the resulting effective heat of ablation for subsonic turbulent flow was found to be

$$H_{eff} = c_p T_v + h_v + 0.55 M^{0.57}(h_e - h_w) \qquad (4)$$

Since the time-distance history of the model can be determined, the ablation on the model can be calculated from a general equation of the form

$$\frac{\Delta m}{m} = \frac{1}{m} \int_o^t \int_S \frac{q_o}{H_{eff}} \, dS \, dt \qquad (5)$$

once values of $q_o$ and $H_{eff}$ are known or given over the trajectory and over the model. Values of $q_o$ were calculated from the model velocity and the simulator channel air properties. The stagnation heat-transfer rates were calculated as suggested in reference 5. The turbulent heat-transfer rate at the spherical tangent point was calculated by the

method given in reference 7. The variation of the heat-transfer rate from the stagnation point to the tangent point was assumed to be linear as suggested in reference 7. The turbulent heat-transfer rates on the conical portion of the model were obtained on the assumption that they were inversely proportional to the one-fifth power of the distance along the surface.

In the present case the inverse problem of equation (5) had to be solved; that is, the equation for $H_{eff}$ was assumed in the form of equation (4) and the numerical values in the equation were chosen so that the ablation loss calculated from equation (5) fit the experimental data. In figure 12 there are shown the results of this correlation for turbulent flow on the model. The effective heat of ablation thus obtained is given by the equation

$$H_{eff} = 1100 + 0.37(h_e - h_w) \frac{Btu}{lb} \qquad (6)$$

In the calculation, $h_w$ was assumed negligible compared to $h_e$ and the flow on the model was assumed to be turbulent throughout the entire trajectory. Estimates of the error introduced by disregarding the conjectured partial laminar ablation in the initial part of the trajectory have been made. At the entry velocity of 14,000 feet per second, the error was about 10 percent but it decreases rapidly with increasing entry velocity.

The first term of equation (6), which is the heat capacity of the material, is in good agreement with the estimated values of the heat capacity for hydrocarbon plastics. When equations (4) and (6) are compared there can be obtained a molecular weight of 58 for ethyl cellulose vapor. It may be noted then that if an effective heat of ablation had been determined by the above method for laminar flow conditions over the trajectory, the numbers obtained would be physically absurd.

When equation (6) was employed, only the data for entry stagnation enthalpies of 3,900 Btu per pound ($V_E$ = 14,000 ft/sec) and above were used in the curve-fitting process. But, as is noticed, the resulting curve passed very nearly through the data for an entry stagnation enthalpy of 2,000 Btu per pound ($V_E$ = 10,000 ft/sec) where laminar flow was assumed to exist. This may be a result of the unsuspected presence of turbulent flow or other factors which might be significant at these low velocities. Further study will be needed to resolve this question.

## CONCLUDING REMARKS

The Ames atmosphere entry simulator has been described and its application to the study of the ablative properties of materials has been presented. The tests simulated the motion, heating, and ablation losses of missiles which enter the atmosphere at velocities from 10,000 to 21,500 feet per second. For the nose shape and material tested, the results indicated that the ablation losses varied from 0.5 to 2.6 percent of the initial weight of the simulated missile as the entry velocity increased. In addition, the results indicated that this material could withstand the thermal stresses associated with these entry conditions. On the basis of these results, it was concluded that the material tested, ethyl cellulose, may be a reasonably efficient ablative material for long-range ballistic missiles of the type simulated.

On the basis of various considerations, it was concluded that the boundary-layer flow over the nose was predominantly turbulent at the higher entry velocities. The experimental ablation losses were therefore employed in conjunction with an expression for the effective heat of ablation in turbulent flow to estimate the ablative properties of ethyl cellulose.

Ames Research Center
National Aeronautics and Space Administration
Moffett Field, Calif., July 5, 1960

# APPENDIX A

## SYMBOLS

| | |
|---|---|
| $A$ | maximum cross-section area of model or missile, sq ft |
| $c_p$ | specific heat of ablative material, Btu/lb-$^{o}$F |
| $C_D$ | drag coefficient of model or missile, dimensionless |
| $h_e$ | local specific enthalpy, Btu/lb |
| $h_v$ | latent heat of vaporization, Btu/lb |
| $h_w$ | specific enthalpy corresponding to vaporization temperature, Btu/lb |
| $H_{eff}$ | effective heat of ablation, $\frac{q_o}{w}$, Btu/lb |
| $m$ | mass, slugs |
| $M$ | molecular weight ratio of air to material vapor, dimensionless |
| $q_o$ | heat-transfer rate to a nonablating surface, Btu/ft$^2$ sec |
| $q_i$ | heat-transfer rate to an ablating surface, Btu/ft$^2$ sec |
| $q_t$ | stagnation heat-transfer rate, Btu/ft$^2$ sec |
| $R_\infty$ | free-stream Reynolds number based on spherical tip radius, dimensionless |
| $R_x$ | local Reynolds number at the tangent point of the spherical tip, dimensionless |
| $S$ | surface area of the model nose, sq ft |
| $t$ | time |
| $T_v$ | vaporization temperature, $^{o}$F |
| $V$ | velocity of model or missile relative to air stream, ft/sec |
| $V_a$ | velocity of model relative to simulator nozzle, ft/sec |
| $V_E$ | entry velocity of missile or initial velocity of model relative to air stream, ft/sec |

$V_m$ muzzle velocity of model, ft/sec

$V_s$ velocity of air stream in simulator, ft/sec

w rate of ablation or mass injection into the boundary layer, $lb/ft^2/sec$

y distance along simulator nozzle or altitude, ft

$\beta$ density distribution constant in simulator, 1/ft

$\rho$ local density, slugs/cu ft

$\rho_o$ density in reservoir, slugs/cu ft

## APPENDIX B

## METHOD FOR DETERMINING ENTRY VELOCITY IN THE SIMULATOR

The ballistic velocity equation given in reference 1 is, when applied to the simulator, slightly in error because of the presence of a small but not completely negligible air-stream velocity in the simulator channel. For the purpose of determining the velocity in the channel, it is worthwhile to refine the velocity equation by taking into account the stream velocity.

With the frame of reference taken as the channel and with the positive direction taken downstream toward the model launcher, the equation of motion of the model becomes

$$mV_a \frac{dV_a}{dy} = \frac{C_D \rho A}{2} (V_a+V_s)^2 \qquad (B1)$$

A closed integral of this equation is not available. However, an approximate solution of this equation leads to a means for correlating experimental measurements. The stream velocity, $V_s$, is, in general, small compared to the model velocity, $V_a$; hence the term $V_s^2$ is neglected, giving

$$\frac{1}{V_a} \frac{dV_a}{dy} = \frac{C_D \rho A}{2m} \left(1+2 \frac{V_s}{V_a}\right) \qquad (B2)$$

The term $V_s/V_a$ is reasonably constant in the simulator. Therefore $V_s$ and $V_a$ in the term $2V_s/V_a$ can be replaced by their respective values at the large end of the channel; namely $V_s$ = 2380 feet per second and $V_a = V_m$.

Equation (B2) can now be easily integrated (employing eq. (1) in the text) to yield

$$\log \frac{V_a}{V_m} = - \frac{C_D \rho_o A}{2m\beta} \left(1 + \frac{4760}{V_m}\right) e^{-\beta y} \qquad (B3)$$

where for simplicity the boundary condition $V_a = V_m$ at $y = \infty$ is used. Note that this equation is equivalent to the velocity equation given in reference 1, except for the term $4760/V_m$, and that $V_a$ refers not to the relative velocity between the air and the model but to the absolute velocity of the model in the simulator channel. It is seen

from equation (B3) that a plot of $V_a$ as a function of $e^{-\beta y}$, or its equivalent $\rho/\rho_o$, on semilogarithmic paper should be a straight line. Figure 13 shows such a plot for a typical test run. The straight line through the experimental points can be extrapolated accurately to the entrance end of the channel as indicated in this figure.

## APPENDIX C

## DERIVATION OF EFFECTIVE HEAT OF ABLATION FOR TURBULENT FLOW

The analysis for turbulent flow follows the same pattern as the one for laminar flow given in reference 9. Thus, the heat capacity of the ablating material, which includes the energy of vaporization, is given by

$$\frac{q_i}{w} = c_p T_v + h_v \tag{C1}$$

In reference 9 the relation between the heat-transfer rates with and without mass injection was obtained from laminar transpiration cooling theory. In the turbulent case, experimental results are used since theory is not at present reliable. In reference 10 results with gas injection are given for skin-friction measurements but these can be interpreted approximately for heat-transfer results by the application of Reynolds analogy. Thus, the variables used in reference 10 can be transformed as follows:

$$\frac{C_F}{C_{F_o}} = \frac{q_i}{q_o} \tag{C2}$$

$$\frac{2F}{C_{F_o}} = \frac{w(h_e - h_w)}{q_o} \tag{C3}$$

Since the flow over the present body shape is, in all probability, subsonic because of the large cone angle, the correlation is made for the case where the surface Mach number is 0.7 (fig. 9(b) in ref. 10). These data are shown replotted in figure 14 in the variables given in equations (C2) and (C3). The simplified empirical formula that appears to best correlate these data is

$$\frac{q_i}{q_o} = 1 - 0.55 \frac{M^{0.57} w(h_e - h_w)}{q_o} \tag{C4}$$

The curves obtained by means of the above expression are also shown in figure 14 to indicate the degree of correlation. Substitution of equation (C4) into equation (C1) together with the definition for $H_{eff}$ gives the desired expression for the effective heat of ablation in the presence of turbulent flow; namely,

$$H_{eff} = c_p T_v + h_v + 0.55 M^{0.57}(h_e - h_w) \tag{C5}$$

REFERENCES

1. Eggers, A. J., Jr.: A Method for Simulating the Atmospheric Entry of Long-Range Ballistic Missiles. NACA Rep. 1378, 1958. (Supersedes NACA RM A55I15)

2. Neice, Stanford E., Carson, James A., and Cunningham, Bernard E.: Experimental Investigation of the Simulation of Atmospheric Entry of Ballistic Missiles. NACA RM A57I26, 1957.

3. Bowman, Gary H., and Savin, Raymond C.: An Experimental Investigation in an Atmosphere Entry Simulator of Nylon as an Ablation Material for Ballistic Missiles. NASA TM X-114, 1959.

4. Bioletti, Carlton, and Cunningham, Bernard E.: A High-Velocity Gun Employing a Shock-Compressed Light Gas. NASA TN D-307, 1960.

5. Kemp, N. H., and Riddell, F. R.: Re-entry Heat Transfer to Satellite Vehicles. Jet Propulsion, vol. 27, no. 2, pt. 1, Feb. 1957.

6. Eggers, A. J., Jr., Allen, H. Julian, and Neice, Stanford E.: A Comparative Analysis of the Performance of Long-Range Hypervelocity Vehicles. NACA Rep. 1382, 1958. (Supersedes NACA TN 4046)

7. Lees, L.: Similarity Parameters for Surface Melting of a Blunt Nosed Body in a High Velocity Gas Stream. A.R.S. Jour., May 1959.

8. Seiff, Alvin, Sommer, Simon C., and Canning, Thomas N.: Some Experiments at High Supersonic Speeds on the Aerodynamic and Boundary Layer Characteristics of High-Drag Bodies of Revolution. NACA RM A56I05, 1957.

9. Georgiev, Steven, Hidalgo, Henry, and Adams, Mac C.: On Ablation For the Recovery of Satellites. Avco Research Laboratory, Research Report 47, March 6, 1959.

10. Pappas, Constantine C., and Okuno, Arthur F.: Measurements of Skin Friction of the Compressible Turbulent Boundary Layer on a Cone With Foreign Gas Injection. Jour. Aero/Space Sci., vol. 27, no. 5, May 1960, pp. 321-333.

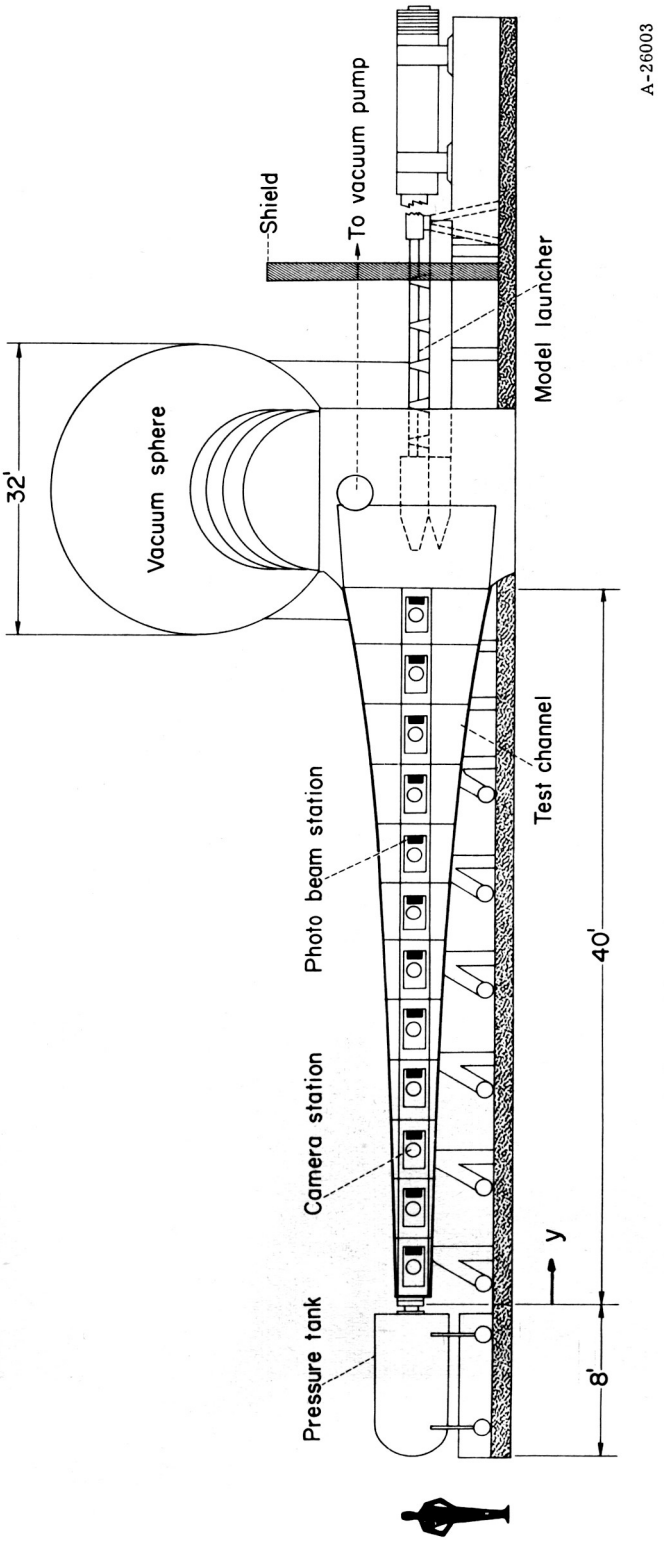


Figure 1.- Schematic diagram of the Ames Atmosphere Entry Simulator.

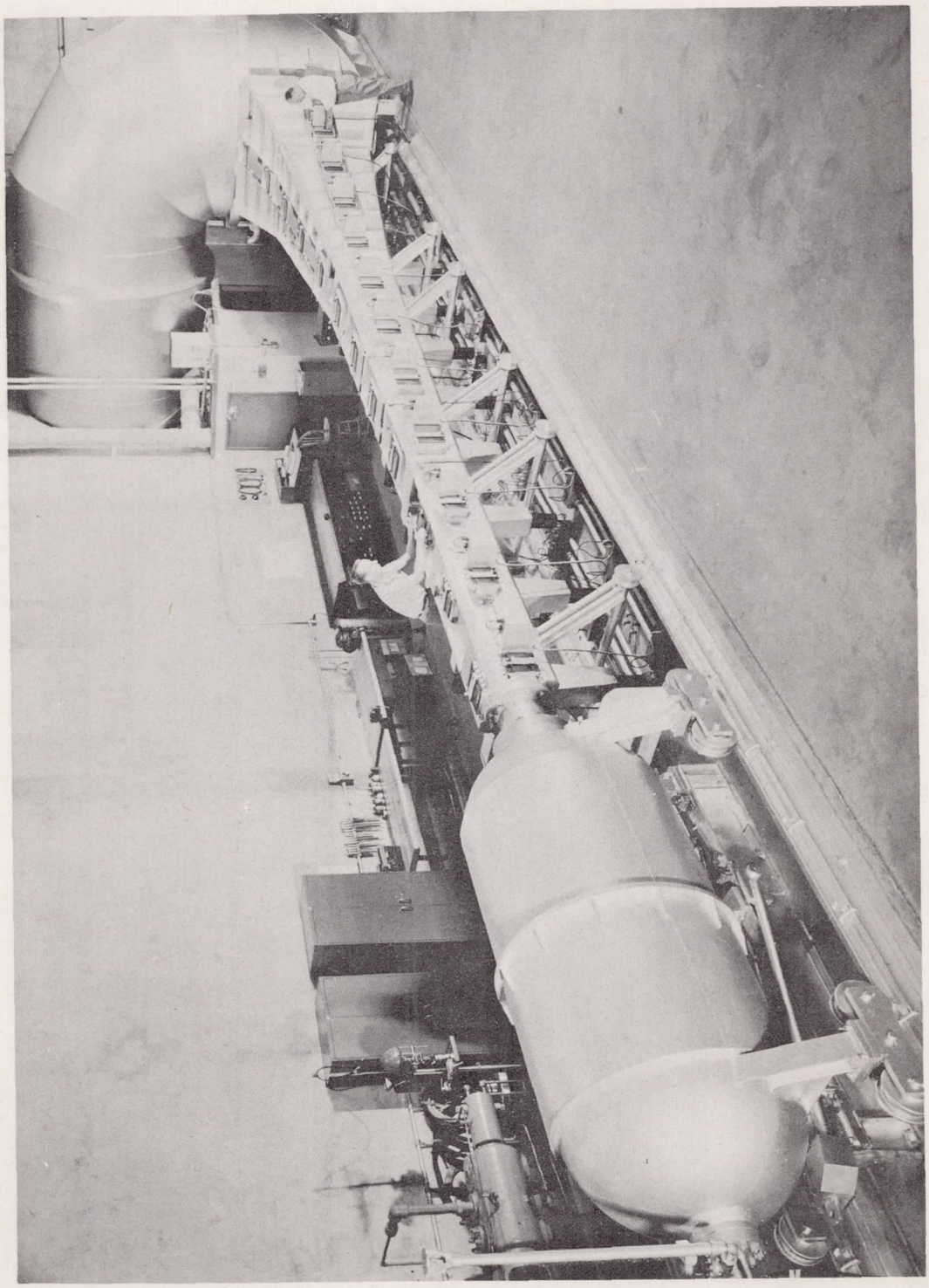

A-24013

Figure 2.- The Ames Atmosphere Entry Simulator.

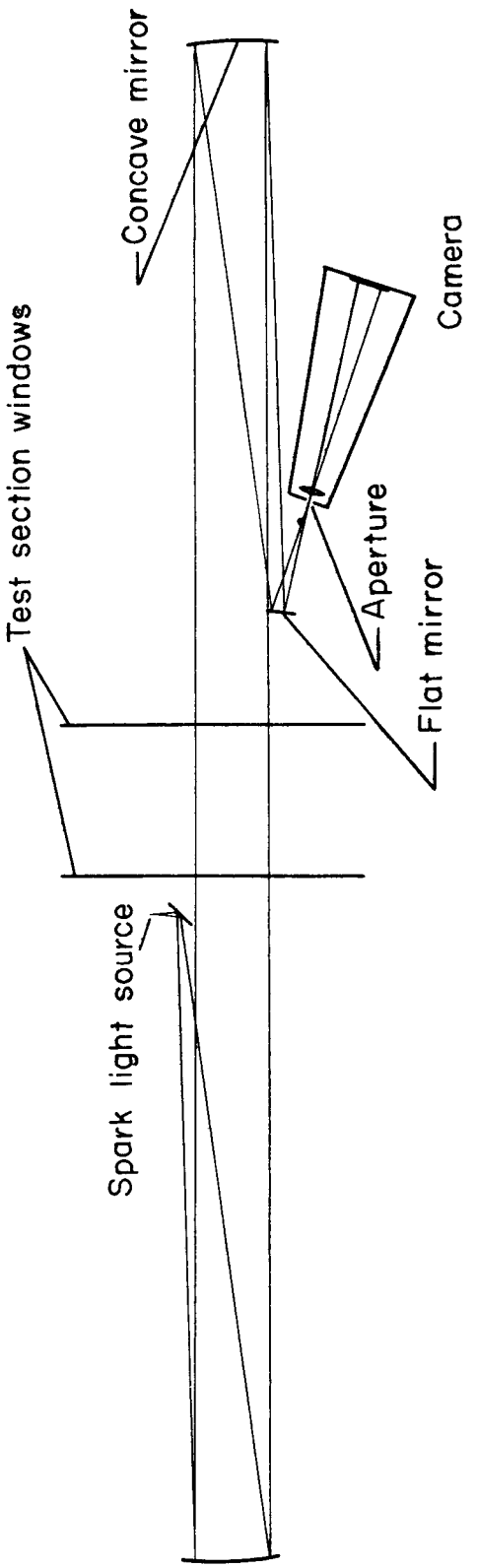


Figure 3.- Schematic diagram of the shadowgraph optical system.

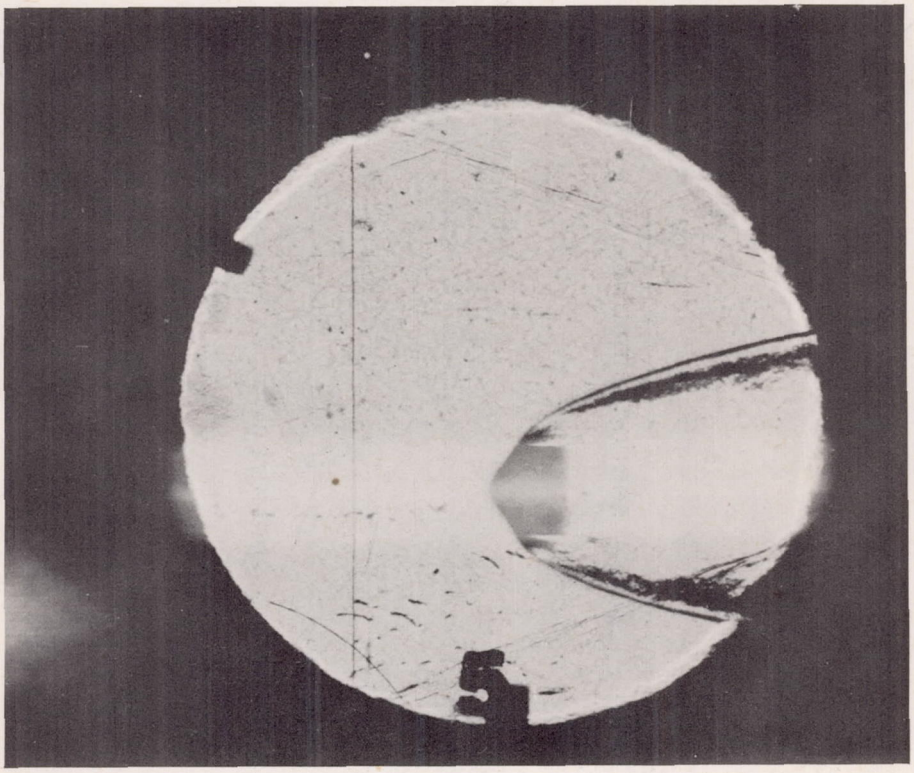

Model velocity – 19,000 ft/sec

Figure 4.- Typical shadowgraph of a model in flight in the simulator.

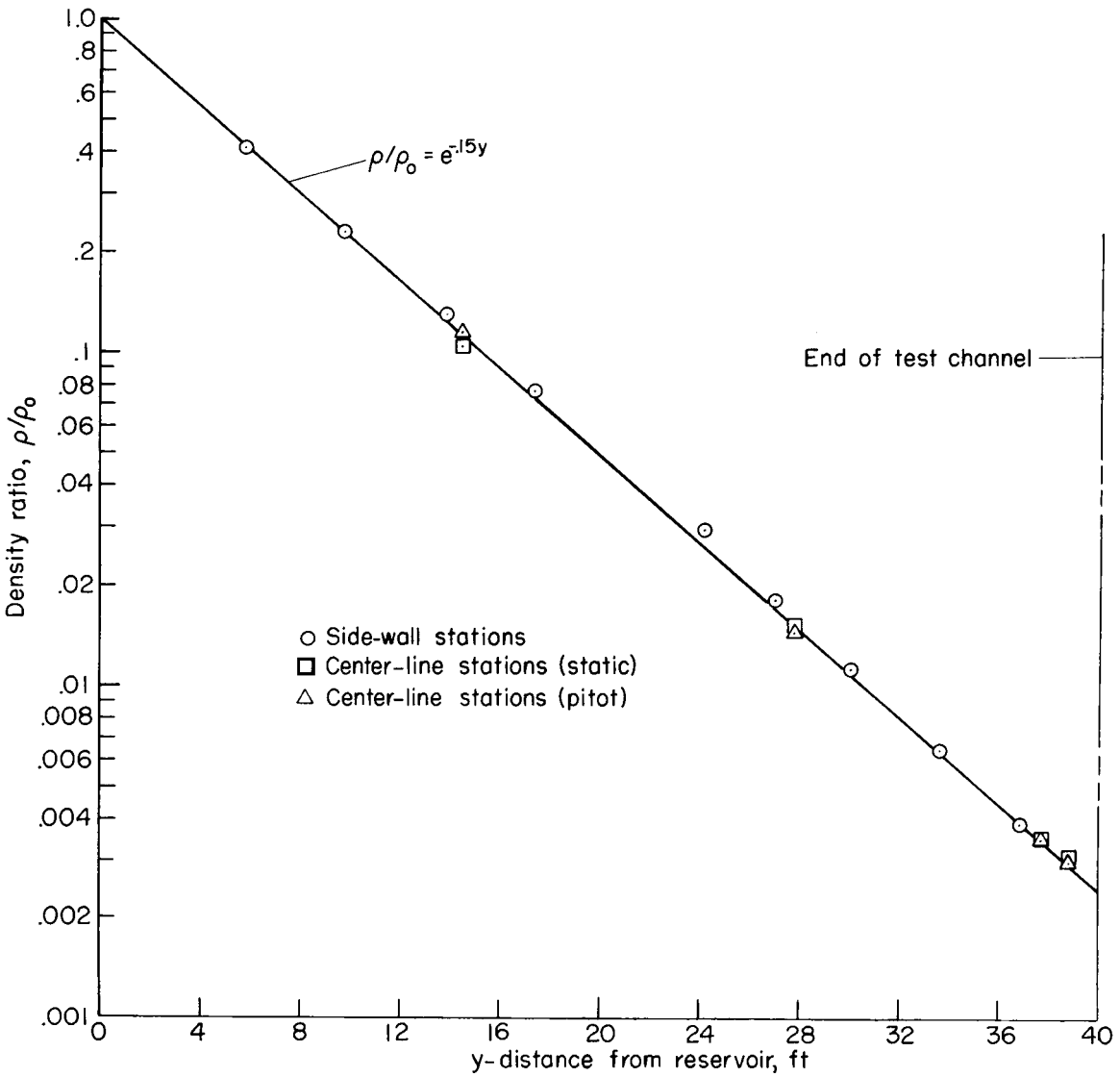


Figure 5.- Variation of density ratio with test section length.

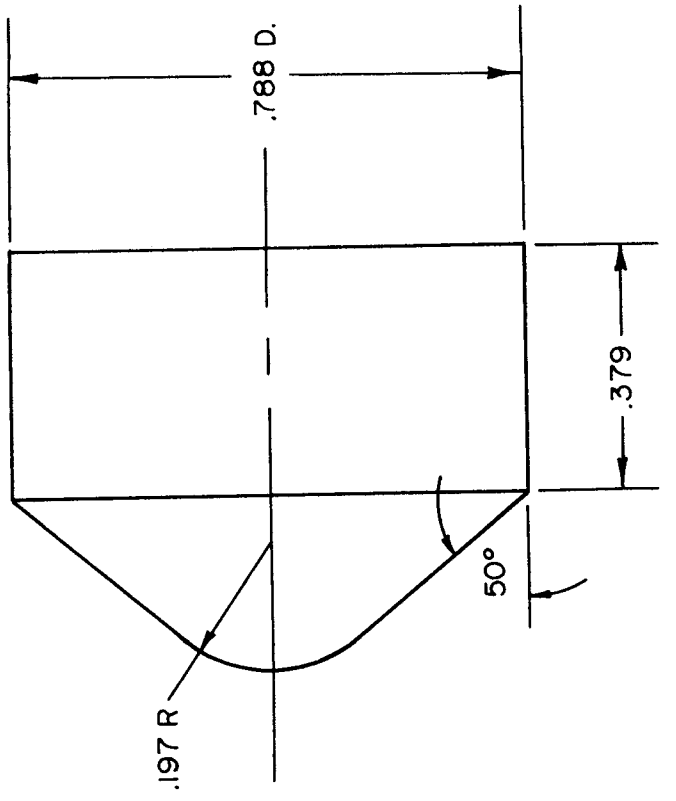


Note: All dimensions in inches.

Figure 6.- Dimensions of test models.

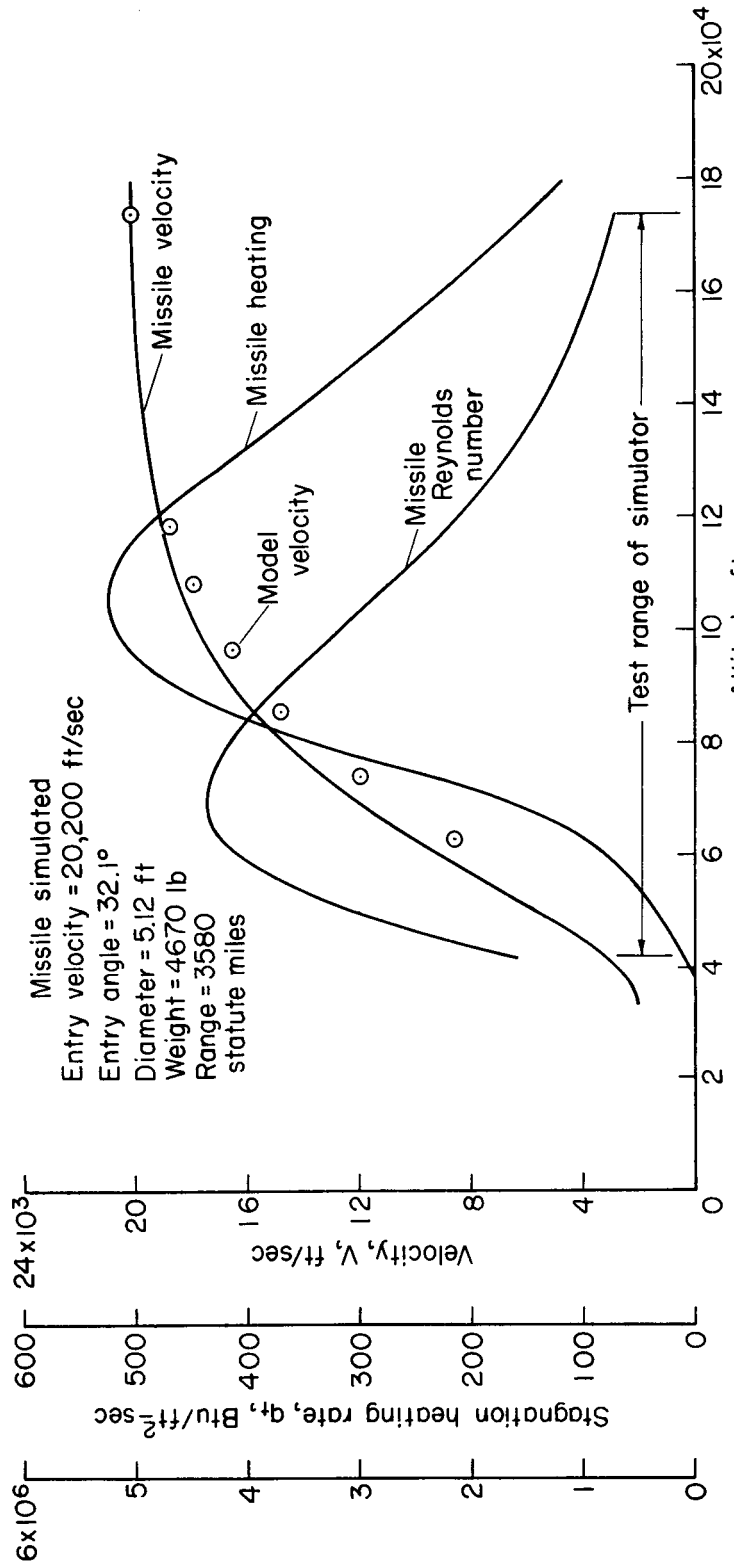


Figure 7.- Variation of velocity, stagnation heating rate and missile Reynolds number with simulated altitude.

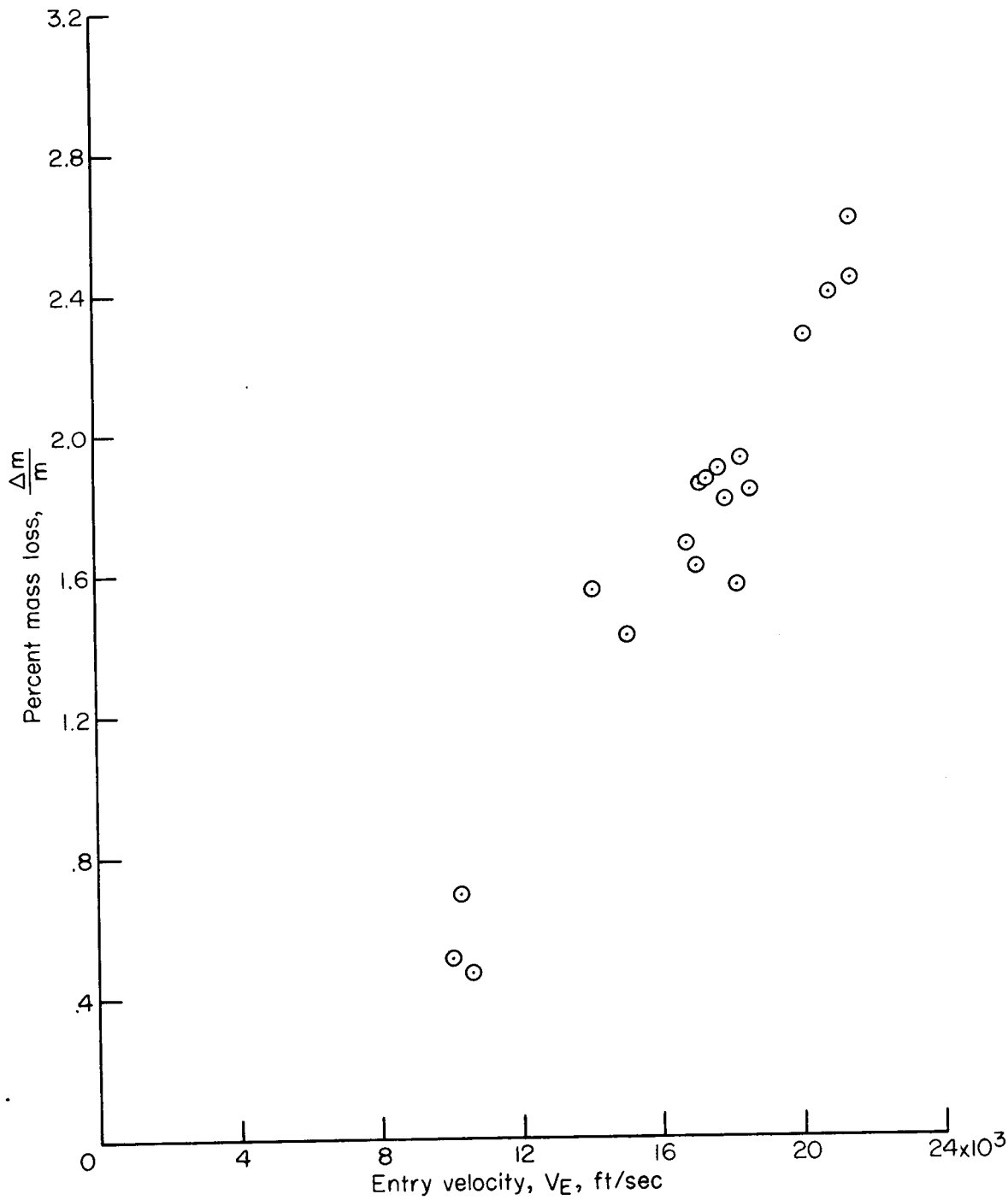


Figure 8.- Variation of ablation mass loss with entry velocity.

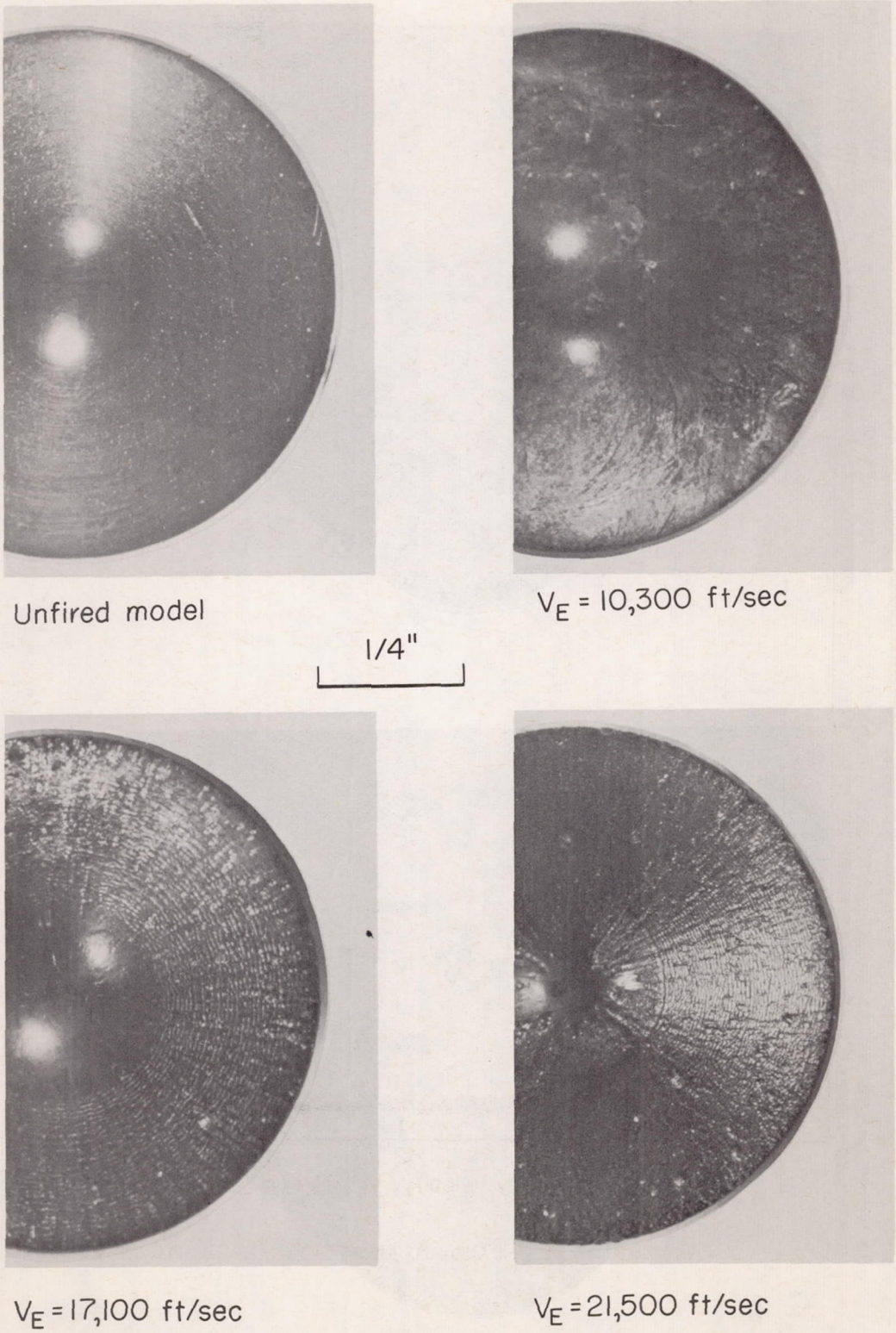


Figure 9.- Photographs of model surfaces.

(a) $V_E$ = 10,300 ft/sec



(b) $V_E$ = 21,500 ft/sec

Figure 10.- Profiles of ablated models compared with the original shapes.

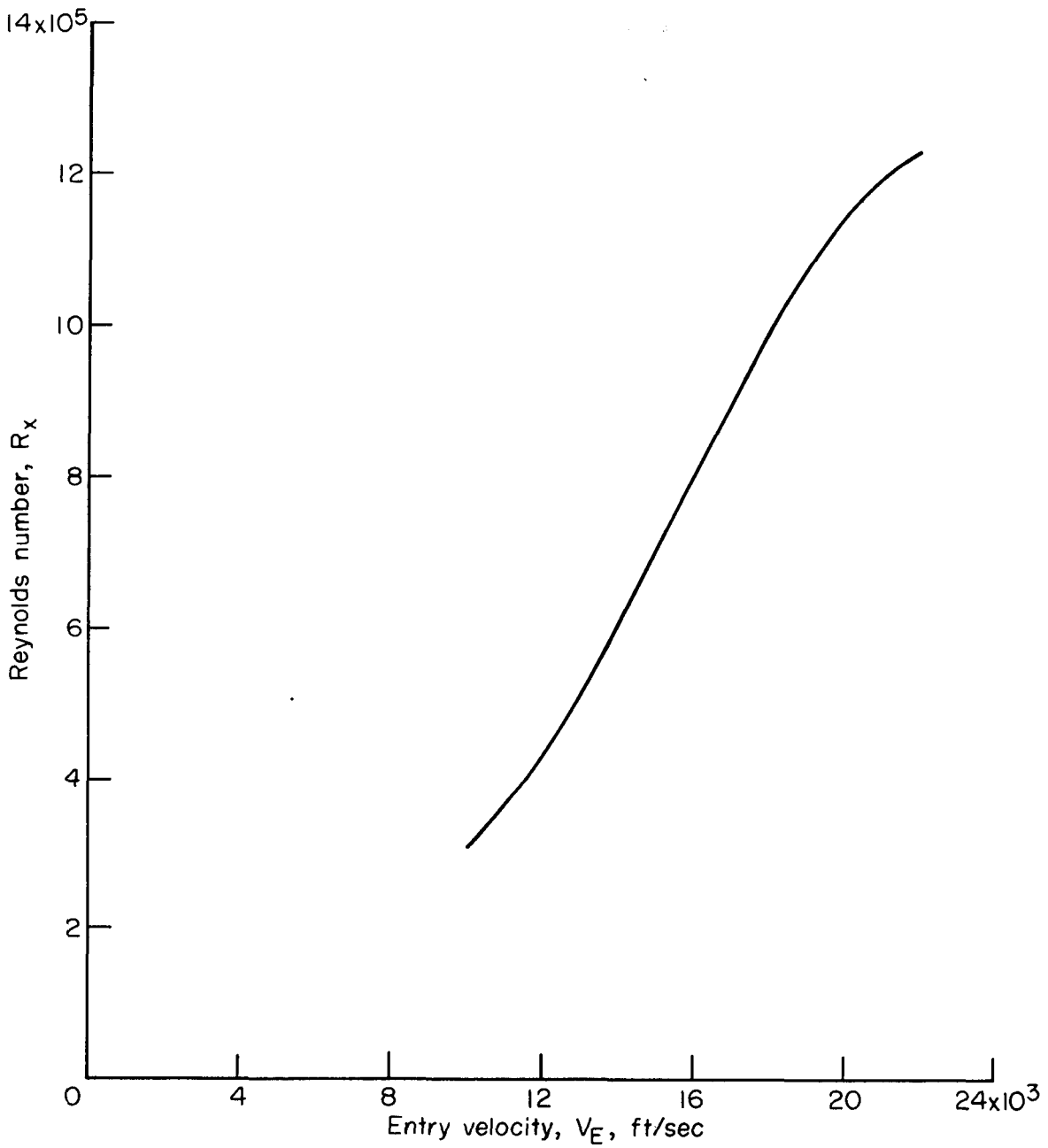


Figure 11.- Variation with entry velocity of local Reynolds number on the model at the tangent point of the spherical tip for the point of maximum heating.

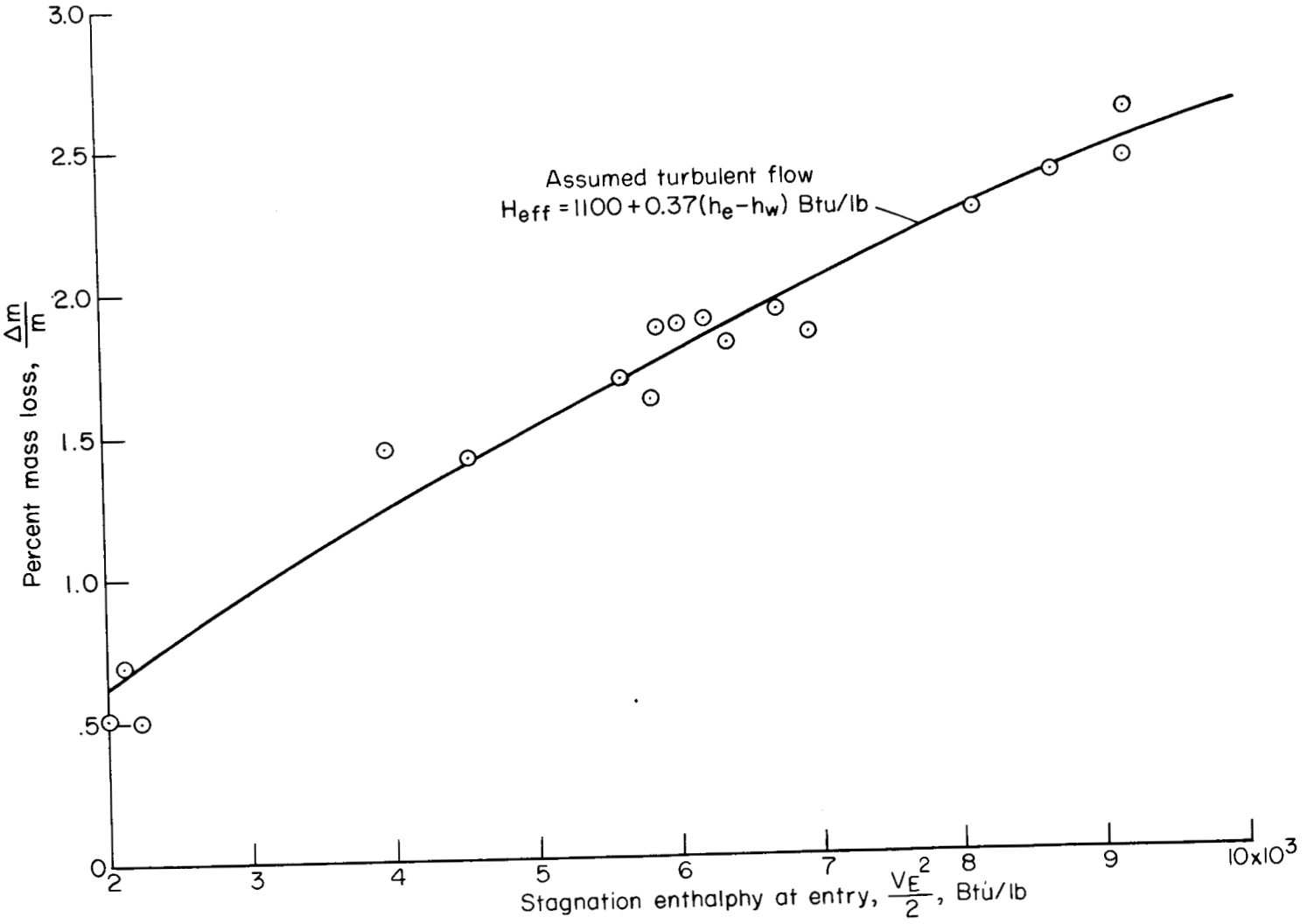


Figure 12.- Comparison of theoretical and experimental ablation mass loss.

CONFIDENTIAL

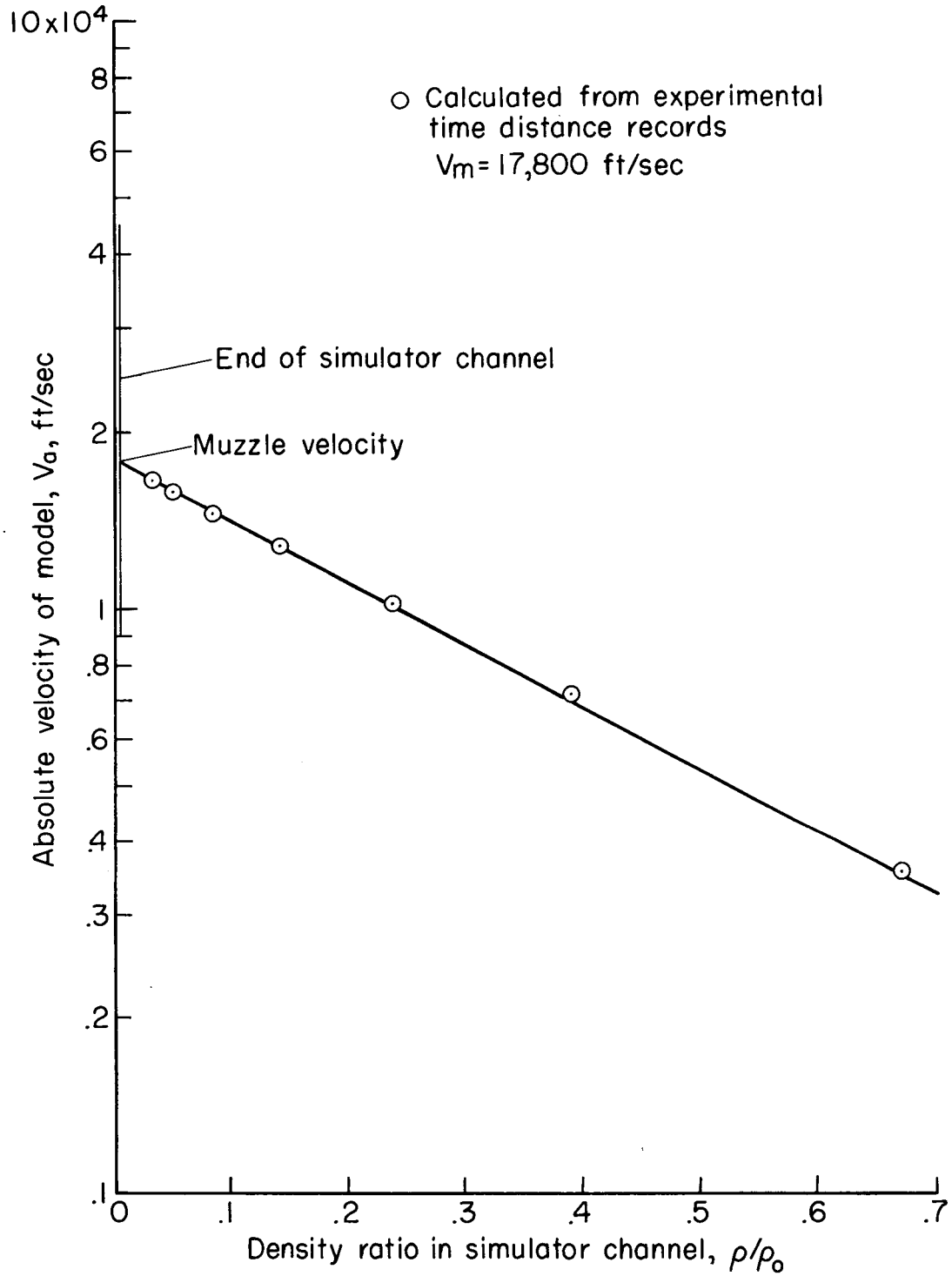


Figure 13.- Variation of model velocity with air density ratio in the simulator channel.

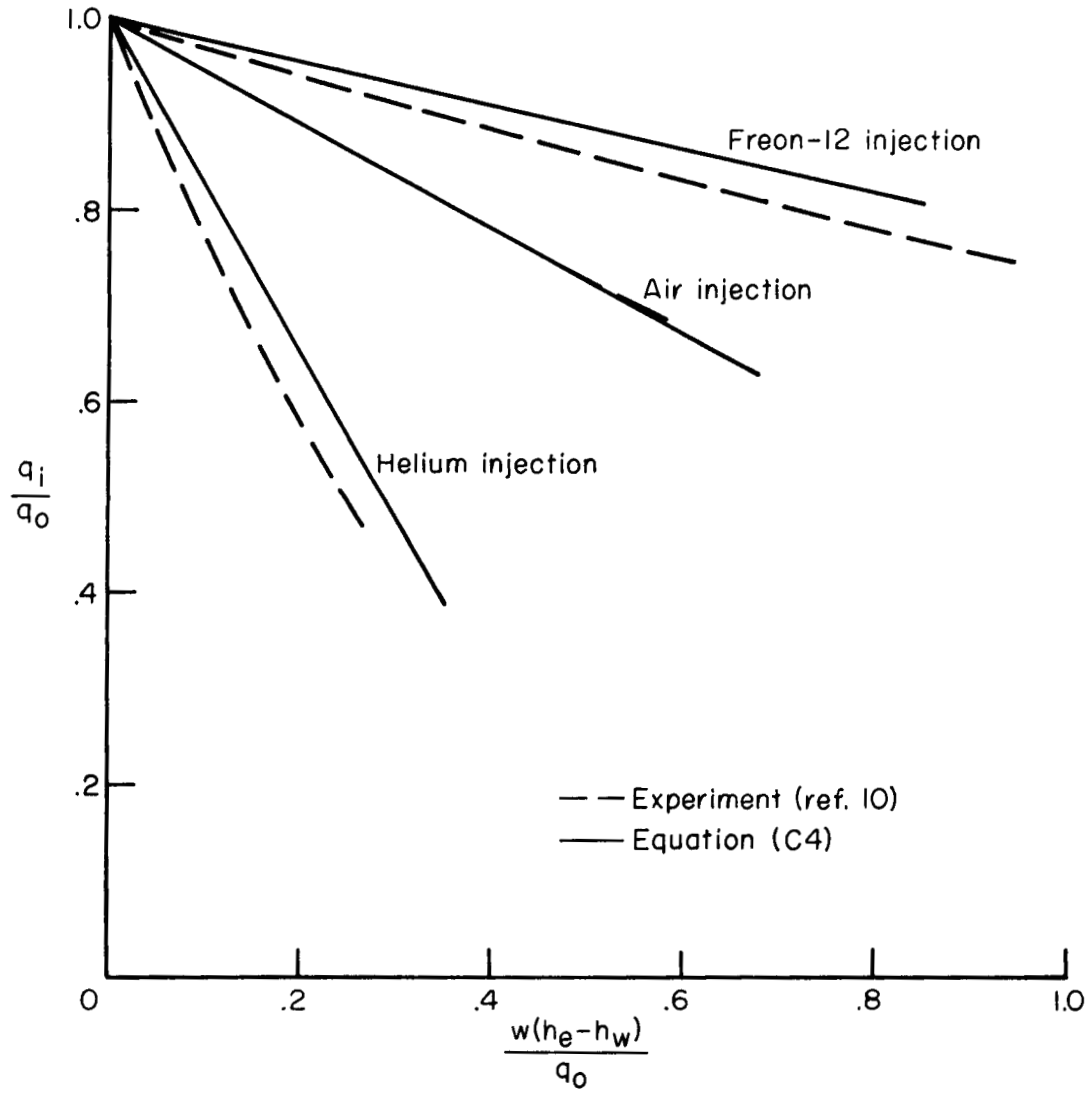


Figure 14.- Correlation of experimental results for reduction of heat-transfer rate by vapor injection.



NASA - Langley Field, Va. A-356